IMPLEMENTATION AND VALIDATION OF A NUMERICAL MODEL FOR LEAD-RUBBER SEISMIC ISOLATION BEARINGS

T. Zhou **Y. F. Wu**

School of Civil Engineering
Southeast University
Nanjing, China

A. Q. Li*

School of Civil Engineering
Southeast University
Nanjing, China

Beijing Advanced Innovation Center for Future Urban Design
Beijing University of Civil Engineering and Architecture
Beijing, China

ABSTRACT

This paper presents a numerical model for accurately representing the behaviors of lead-rubber bearings during earthquakes. This model, which is implemented in OpenSees as a user-defined element, accounts for the mechanical characteristics of bearings as follows: firstly, the bi-lateral interaction effect of hysteretic behaviors, as well as the variation in horizontal stiffness due to vertical load, is considered; secondly, the reduced vertical stiffness under large lateral displacement is incorporated by the piecewise linear formulation, and the linear reduction method is employed to determine the stability limit of bearings in the deformed configuration; furthermore, the cavitation and permanent damage effects in bearings are mathematically included. To validate the numerical model, simulation analyses are performed for a series of static and dynamic loading tests, and the numerical results show reasonable agreement with experimental ones, which indicates that the proposed model provides an effective tool for the failure mode analyses of bearings and the dynamic analyses of seismic isolated structures.

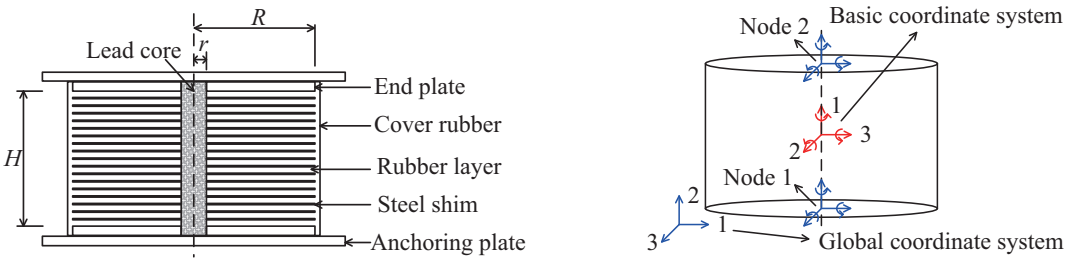
Keywords: Lead-rubber bearings, Bidirectional interaction effect, Critical load, Tensile behavior.

1. INTRODUCTION

The effectiveness of seismic isolation technique for seismic protection of new structures and seismic retrofitting of existing ones has been confirmed, consequently, it has been extensively employed in buildings, bridges, nuclear power plants and so forth [1-3]. The seismic inertial forces can be effectively reduced by the introduction of isolators that are vertically relatively stiff but horizontally flexible. The common use of lead-rubber bearings (LRBs) has necessitated a further understanding of its mechanical behaviors. Chalhoub *et al*. [4] proposed the pressure solution (PS) method to theoretically derive the vertical stiffness of bearings with rigid reinforcements, in which the bulk compressibility was taken into account. This method was then extended by Tsai [5] to analyze the compression and bending stiffness of laminated elastic materials bonded to flexible reinforcements, which was hereafter known as the pressure approach (PA) method. Huang [6] experimentally investigated the bidirectional interaction response of LRBs subjected to bi-lateral static and dynamic loadings. Harvey *et al*. [7] presented a bidirectional hysteretic model in which the smoothness from elastic to yield state could be modified without influencing the isotropic yield surface. Warn *et al*. [8] experimentally evaluated four formulations for predicting the reduced vertical stiffness due to lateral displacement, which included the two-spring model, the tension buckling formulation, the overlapping area method and the piecewise linear method. The test results revealed that the piecewise linear method matched the experimental results with the least residual errors. Weisman *et al*. [9] experimentally and numerically studied the critical load of bearings at large horizontal displacement, and found that the overlapping area method conservatively estimated the reduction in critical load. Sanchez *et al*. [10] experimentally examined the stability limit of bearings under two quasi-static loadings and one dynamic loading, and found that the quasi-static loading results agreed well with the dynamic

* Corresponding author (220150981@seu.edu.cn)

DOI : 10.1017/jmech.2017.100
Copyright © 2017 The Society of Theoretical and Applied Mechanics
https://doi.org/10.1017/jmech.2017.100 Published online by Cambridge University Press



(a) Sectional view of the bearing (b) Element coordinate system

Fig. 1 Numerical model for circular LRBs.

loading ones. Kumar *et al*. [11] experimentally investigated the tensile behavior of bearings. The results revealed that the tension stiffness was reduced due to the cavitation in rubbers, and the reduction in cavitation strength depended on the previous maximum tensile displacement. Crowder *et al*. [12] studied the influence of support rotation on mechanical responses of bearings, and found that the horizontal stiffness was remarkably reduced due to the flexible end conditions. Tubaldi *et al*. [13] parametrically studied the potential buckling failure or uplift effect in bearings on which excessive compressive loads, or even tensile loads, may act under seismic excitations.

With regard to the mechanical models for LRBs, Koh and Kelly [14] presented a simple linear two-spring model to account for axial-shear interaction. Ryan *et al*. [15] then extended the two-spring model by introducing a nonlinear shear spring. Yamamoto *et al*. [16] and Kikuchi *et al*. [17] developed the multi-spring models for circular and square bearings, respectively. Subsequently, Ishii *et al*. [18] extended the multi-spring model to describe the responses of bearings subjected to combined shear deformation and end rotation. Kumar *et al*. [19] presented a mathematical model that included the horizontal-vertical interaction effect by the two-spring model, meanwhile, nonlinear tensile behaviors were reasonably characterized by the model. Han *et al*. [20] developed a model that employed a series of vertical springs to describe nonlinear rotational responses instead of a single concentrated rotational spring. Maureira *et al*. [21] presented a mathematical model derived from both the kinematics of single rubber layer and the co-rotational formulation, this model could capture the global response of bearings and the local strain and stress field of each rubber layer.

In current software programs, such as SAP2000, PERFORM-3D and 3D-BASIS [22], a linear spring is typically utilized to represent the axial characteristic of bearings with the option to provide different values of stiffness in compression and tension, and the bilinear model or the modified Bouc-Wen model (i.e., the Park model [23]) is employed to describe nonlinear hysteretic behaviors of bearings in the horizontal plane. As mechanical properties of bearings may change substantially, especially under moderate to major earthquakes, the bearing elements in current software programs are unable to accurately predict the performance of LRBs. In view of the limitations of current bearing elements, a numerical model of LRBs is presented in this study and implemented in OpenSees [24] as a new user-defined element. This model is capable of representing the following behaviors of bearings simultaneously: the bidirectional interaction effect in horizontal directions; the variation in horizontal stiffness due to vertical load; the reduced vertical stiffness and critical load with increasing lateral offset; and the cavitation and permanent damage effects under tension. Simulation analyses are conducted for both static and dynamic loading tests to evaluate the rationality of model parameters in the proposed model and to demonstrate the performance of LRBs when considering the variation in mechanical properties.

2. THE NUMERICAL MODEL FOR LEAD-RUBBER BEARINGS

The numerical model for circular LRBs (Fig. 1(a)) is considered as a three-dimensional macro element with two nodes and twelve degrees of freedom (Fig. 1(b)), and the mechanical characteristics along each direction in the basic coordinate system are presented in the following subsections.

2.1 Bi-Lateral Hysteretic Behaviors

The Bouc-Wen model [25] is typically adopted to describe hysteretic responses of some nonlinear components and devices, and the studies devoted to this model mainly focus on parameter identification, analysis, modeling, control and so forth [26]. The uniaxial Bouc-Wen hysteretic model [27] was generalized by Park *et al*. [23] to consider the bidirectional interaction effect, and the bidirectional Park model has been extensively utilized to simulate hysteretic behaviors of bearings in existing FEA software programs. However, the independence of loading/unloading conditions in the horizontal plane in this model is inconsistent with the assumption of isotropic response for circular bearings, so the modified bidirectional Bouc-Wen model proposed by Casciati [28] is utilized in the following.

In the model, the horizontal resisting force $F=\left[F_x \;\; F_y\right]^T$ of bearings is determined by the following equations:

https://doi.org/10.1017/jmech.2017.100 Published online by Cambridge University Press

$$\begin{bmatrix} F_x \\ F_y \end{bmatrix} = K_d \begin{bmatrix} U_x \\ U_y \end{bmatrix} + Q_d \begin{bmatrix} Z_x \\ Z_y \end{bmatrix} + c_b \begin{bmatrix} \dot{U}_x \\ \dot{U}_y \end{bmatrix} \quad (1)$$

where $U = [U_x\ U_y]^T$ is the horizontal deformation vector with two orthogonal components U_x and U_y; K_d is the post-elastic stiffness; Q_d is the characteristic strength; c_b is the viscous damping coefficient of rubbers and is typically neglected in LRBs; $Z = [Z_x\ Z_y]^T$ is a dimensionless hysteretic variable that satisfies the first-order differential equations as follows:

$$Y \begin{bmatrix} \dot{Z}_x \\ \dot{Z}_y \end{bmatrix} = \left(A[I] - \chi \begin{bmatrix} Z_x^2 & Z_x Z_y \\ Z_x Z_y & Z_y^2 \end{bmatrix} \right) \begin{bmatrix} \dot{U}_x \\ \dot{U}_y \end{bmatrix} \quad (2)$$

and

$$\chi = \|Z\|^{\eta-2} \left[\delta + \beta \operatorname{sign}\left(\dot{U}_x Z_x + \dot{U}_y Z_y \right) \right] \quad (3)$$

in which the yield displacement Y is defined as $Y = Q_d/((\tau - 1)K_d)$, here the parameter τ is the ratio of elastic stiffness to post-elastic stiffness and is taken to be 10 for seismic loads [29]; $[I]$ is the second-order identity matrix; sign() is the sign function; the smoothness parameter η governs the transition from elastic to plastic state; δ, β and A are the parameters determining the shape and scale of hysteretic loop. Under the condition that $A > 0$ and $\beta + \delta > 0$, the hysteretic variable Z is bounded by $\|Z\| \le \sqrt[\eta]{\left(A/(\beta+\delta)\right)}$. As $A = 1$ and $\beta + \delta = 1$, the hysteretic force $F_p = Q_d Z$ traces a circular yield surface, with the hysteretic variable Z bounded by the values of ±1. As referred to the previous studies [26, 30], the values of parameters A, β, δ and η are taken to be 1, 0.5, 0.5 and 2, respectively, in this study.

In the Park model, the loading/unloading conditions are dominated by the term $\operatorname{sign}\left(\dot{U}_i Z_i\right)$, $i = x, y$ and are independent in the x and y direction, which violates the assumed isotropic behavior for circular bearings. Unlike the Park model, the term $\operatorname{sign}\left(\dot{U}_x Z_x + \dot{U}_y Z_y\right)$ in Eq. (2) for the Casciati model represents the rotationally-invariant (i.e., isotropic) capacity [30].

In analytical solutions for vertical behaviors of LRBs, the bearing is typically assumed to be isotropic and homogeneous in the horizontal plane. Therefore, the concept of effective shear modulus G_{eff}, which is affected by the post-elastic stiffness of lead core and is determined by the initial post-elastic stiffness $K_{d,0}$ [31], is utilized to account for the contribution of lead core.

$$G_{eff} = \frac{K_{d,0} T_r}{A_b} \quad (4)$$

in which A_b is the bonded area of rubber; T_r is the total rubber thickness ($T_r = n \times t_r$, where n is the number of rubber layers; t_r is the thickness of single rubber layer).

The reduction in horizontal stiffness due to vertical load is included based on the two-spring model [14] and can be approximated by:

$$K_d = K_{d,0} \left[1 - \left(\frac{P}{P_{cr,0}} \right)^2 \right] \quad (5)$$

where P is vertical load; $P_{cr,0}$ is the critical buckling load of bearings under zero lateral displacement, as discussed hereinafter.

2.2 Behaviors under Vertical Loadings

The relatively low lateral stiffness of bearings is always accompanied by large horizontal displacement in the isolation system under moderate to major earthquakes. Therefore, the reduction in both vertical stiffness and critical load of bearings with increasing lateral offset is incorporated in this study. Furthermore, the effects of cavitation and permanent damage in bearings under tension are mathematically considered.

2.2.1 Behaviors under Compression

As mentioned above, the effective shear modulus G_{eff} (Eq. (4)) is utilized to account for the contribution of lead core to mechanical properties of bearings. The comparisons for the initial vertical stiffness and initial critical load between experimental results and analytical approximations based on shear modulus of rubbers and effective shear modulus of bearings are listed in Tables 1 and 2, respectively, which indicate that the effective shear modulus provides a more reasonable estimate of initial vertical stiffness and critical load.

For a LRB with outer radius R and inner radius r (Fig. 1(a)), the initial vertical stiffness in its laterally undeformed state $K_{v,0}$ is given as follows:

$$K_{v,0} = \frac{E_c A_b}{T_r} \quad (6)$$

where the compression modulus E_c is given by [4].

Table 1 Comparison of vertical stiffness in the undeformed configuration $K_{v,0}$ for experimental and analytical results.

Test number	$K_{v,0}$ (kN/mm) experimental	$K_{v,0}$ (kN/mm) based on G	Error (%)	$K_{v,0}$ (kN/mm) based on G_{eff}	Error (%)
7	138.7	115.8	-16.5	157.1	13.2
8	154.1		-24.8		1.9
11	163.3		-29.1		-3.8

Notes: the experimental data from Warn *et al*. [8].

Table 2 Comparison of critical load in the undeformed configuration $P_{cr,0}$ for experimental and analytical results.

Bearing number	$P_{cr,0}$ (kN) experimental	$P_{cr,0}$ (kN) based on G	Error (%)	$P_{cr,0}$ (kN) based on G_{eff}	Error (%)
11783	537	489.8	-8.79	657.1	18.3
11772	643		-23.8		2.15
11792	587		-16.5		10.7

Notes: the experimental data from Sanchez *et al*. [10].

https://doi.org/10.1017/jmech.2017.100 Published online by Cambridge University Press

$$E_c = \frac{1}{\left(\dfrac{1}{6G_{eff}S_1^2\lambda} + \dfrac{4}{3K}\right)} \tag{7}$$

in which the first shape factor S_1 is calculated for LRBs as $S_1 = (R^2 - r^2)/(2Rt_r)$; the bulk modulus of rubbers K is reasonably assumed to be 2000 MPa; the parameter λ is determined from the bearing geometry according to Eq. (8), and λ is close to 2/3, with r/R approaching 1.

$$\lambda = \frac{R^2 + r^2 - \dfrac{R^2 - r^2}{\ln(R/r)}}{(R-r)^2} \tag{8}$$

The piecewise linear formulation, which has been verified experimentally by Warn *et al* [8], is considered here to calculate the vertical stiffness K_v at the given lateral offset u_h as follows:

$$\frac{K_v}{K_{v,0}} = \begin{cases} 1 - 0.4(u_h/R), & u_h/R \le 2 \\ 0.2 \quad , & u_h/R > 2 \end{cases} \tag{9}$$

In the AASHTO Guide Specifications [32], the stability of a bearing should be demonstrated under maximum-considered earthquake and is assessed using

$$P_{cr} \ge 1.2P_D + P_{SL} + P_{OT} \tag{10}$$

where P_{cr} is the critical buckling load of bearings in the deformed state; P_D, P_{SL} and P_{OT} are the vertical loads due to dead, seismic-live and overturning forces, respectively.

Derived from Haringx theory [33], the critical buckling load under zero horizontal displacement $P_{cr,0}$ is determined according to [34]:

$$P_{cr,0} = \frac{\pi^2 G_{eff}\left(R^2 - r^2\right)^2}{2\sqrt{2}T_r t_r} \tag{11}$$

With regard to the determination of critical load in the deformed configuration P_{cr}, the overlapping area method provides overly conservative prediction of P_{cr}. Montuori *et al*. [35] investigated the effect of the second shape factor S_2, which is defined as $S_2 = 2R/T_r$, on the shear behavior and stability issues of bearings, and presented the linear reduction method to determine the reduced critical load P_{cr}:

$$P_{cr} = P_{cr,0}(1 - \gamma/S_2) \tag{12}$$

where the shear strain γ is calculated as $\gamma = u_h/T_r$.

2.2.2 Behaviors under Tension

As is commonly done, the influence of lead core on the tensile behavior of bearings is neglected. Kumar *et al*. [11, 36] presented a mathematical model to represent the tensile behavior of bearings and it is employed in this study.

As illustrated in Fig. 2, the tensile curve is linear until the formulation of initial cavities in rubbers, and it is assumed that the tension stiffness is equal to the initial compression stiffness. The initial cavitation strength F_c and the corresponding initial cavitation displacement u_c

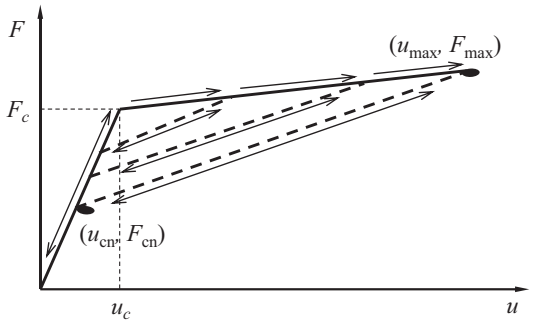


Fig. 2 Illustration of the mathematical model for bearings under tension.

are calculated according to Eq. (13) suggested by Gent [37].

$$F_c = 3GA_b, \quad u_c = F_c/K_{v,0} \tag{13}$$

in which G is the shear modulus of rubbers.

Cavitation in bearings is typically accompanied by the associated tension stiffness reduction, which is manifested by the sharp transition on the tensile curve (Fig. 2). The post-cavitation force is estimated as [36]:

$$F = F_c\left[1 + \frac{1}{kT_r}\left(1 - e^{-k(u-u_c)}\right)\right] \tag{14}$$

where u is the tensile deformation; the cavitation parameter k is used to describe the tensile stiffness reduction in the post-cavitation state.

As shown in Fig. 2, when the tensile deformation exceeds u_c and then unloads, the unloading follows a new path. Subsequently, the loading path coincides with the latest unloading path until the tensile deformation is greater than the previous maximum tensile deformation u_{max}. Upon further loading, there is increasingly irreversible damage in bearings due to the formulation of new cavities, and the post-cavitation behavior follows Eq. (14) defined above. As the reverse loading is applied, it again moves along a new unloading path, which is nearly a straight line between the points of (u_{max}, F_{max}) and (u_{cn}, F_{cn}) (Fig. 2), and the reduced cavitation strength F_{cn} is determined by the u_{max} [36]:

$$F_{cn} = F_c\left(1 - \phi_{max}\left[1 - e^{-\alpha\left(\frac{u_{max} - u_c}{u_c}\right)}\right]\right) \tag{15}$$

in which α is the strength degradation parameter; ϕ_{max} is the damage index. The values of (u_{max}, F_{max}) and (u_{cn}, F_{cn}) change, with the number of cycles increasing.

The values for parameters k, α and ϕ_{max} are required to be calibrated with experimental results, and are taken to be 10, 1 and 0.75, respectively, in this study, as referred to the literatures [11, 36].

2.3 Rotational and Torsional Behaviors

As the mechanical behaviors in rotation and torsion

https://doi.org/10.1017/jmech.2017.100 Published online by Cambridge University Press

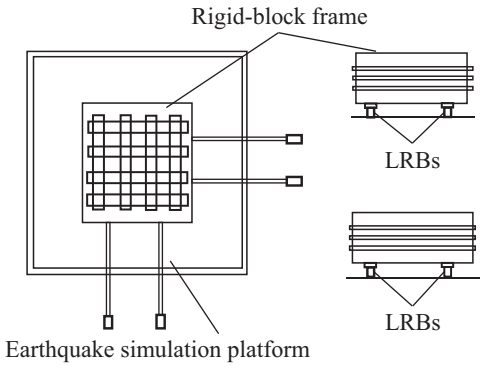


Fig. 3 Plan and elevation schematic of the testing apparatus (Huang [6]).

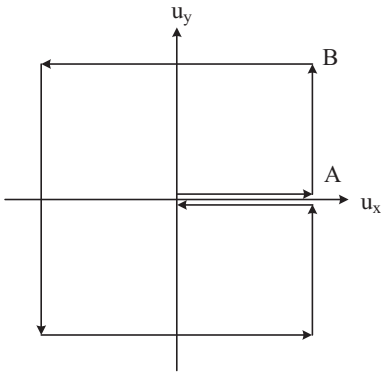


Fig. 4 The box displacement orbit for tests.

slightly affect the responses of bearings, the rotational and torsional stiffness of bearings are assumed to be linear and are given by [34]:

$$K_b = 2G_{eff}S_1^2 I_s\left(1-\frac{3G_{eff}S_1^2}{K}\right)\frac{H}{T_r} \tag{16}$$

$$K_r = \frac{G_{eff}J}{T_r} \tag{17}$$

where I_s, J are the bending moment of inertia and the polar moment of inertia of the bonded area of rubber, respectively; H is the total bearing height excluding end plates (Fig. 1(a)), and the term H/T_r is used to account for the presence of steel shims in the composite system.

3. SIMULATION ANALYSES

In these formulas for mechanical properties of bearings along each direction, the expressions for horizontal and tensile behaviors are based on relatively rigorous theoretical derivations, however, the formulas for the reduction in compression stiffness and critical load in the deformed configuration are empirically obtained from experimental results. Therefore, simulation analyses are conducted for both static and dynamic loading tests to evaluate the applicability of the established model parameters for horizontal and tensile properties in the proposed model. Subsequently, the influence of dimension effect on mechanical behaviors of bearings are numerically investigated by FE bearing models with different sizes. Furthermore, the performances of LRBs are demonstrated when considering the variation in vertical stiffness and critical load.

3.1 Bidirectional Static Tests and Simulation Analyses

The experimental studies of LRBs under bi-lateral displacement histories were conducted by Huang [6] to characterize the bidirectional interaction behavior of bearings. As illustrated in Fig. 3, the rigid-block superstructure was supported by four bearings on the platform. With four steel struts bracing the superstructure against the reaction buttresses off the platform, the platform was then moved along specified bidirectional displacement histories in the horizontal plane. The total weight of the rigid-block test set-up was 289.25 kN.

The bearing had an outer bonded radius of 83.95 mm and an inner radius of 14.98 mm, and it was composed of 19 layers of 3.175 mm thick rubber and 18 layers of 1.905 mm thick steel shim, with the thickness of end plate 12.7 mm. The first shape factor S_1 was 12.8; the second shape factor S_2 was 2.78; the shear modulus of rubbers G was 0.55 MPa; the characteristic strength Q_d was 6.786 kN; and the initial post-elastic stiffness $K_{d,0}$ was 0.1775 kN/mm.

As shown in Fig. 4, the box displacement orbit (γ = 100%) in the horizontal plane was selected in this displacement-control testing.

The experimental and simulated responses of one bearing for the bidirectional tests are shown in Figs 5, 6 and 7. The bidirectional interaction characteristic of LRBs can be obviously illustrated by the resisting force locus plot presented in Fig. 5: with fixed horizontal displacement in the x direction (γ = 100%), the corresponding resisting force in the x direction is reduced due to loading along the y direction (from point A to point B in Figs. 4 and 5). The proposed model, as shown in Fig. 5, can capture the observed force reduction effect of the bidirectional coupled behavior. Nevertheless, in the numerical result, the force interaction curve is nearly a quarter circle, whereas it is an approximate straight line in experiment.

This bidirectional interaction characteristic is consistent with the Casciati model, in which the hysteretic force ($F_p = Q_d \cdot Z$) is coupled through a circular interaction surface. The time history of hysteretic variable Z is shown in Fig. 6, after the first yielding (point A), the simulated hysteretic variable traces a circle. As illustrated in Fig. 7, the simulation responses predicted by the proposed model can match the experimentally observed hysteresis loops in the two orthogonal directions with slight residual errors. Therefore, the established model parameters: A = 1, β = 0.5, δ = 0.5 and η = 2 in this proposed model can effectively characterize the bidirectional coupled behavior of LRBs under bi-lateral static excitation.

https://doi.org/10.1017/jmech.2017.100 Published online by Cambridge University Press

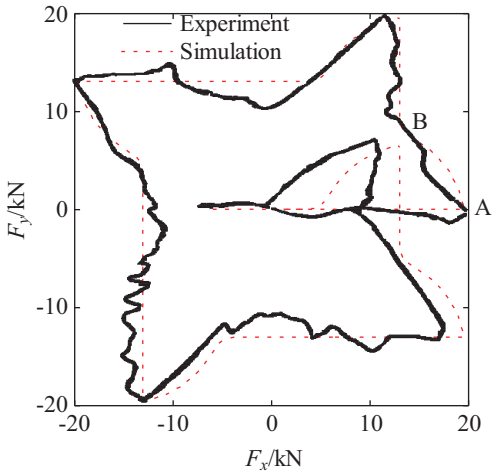


Fig. 5 Comparison of experimental and numerical results for the bidirectional resisting forces.

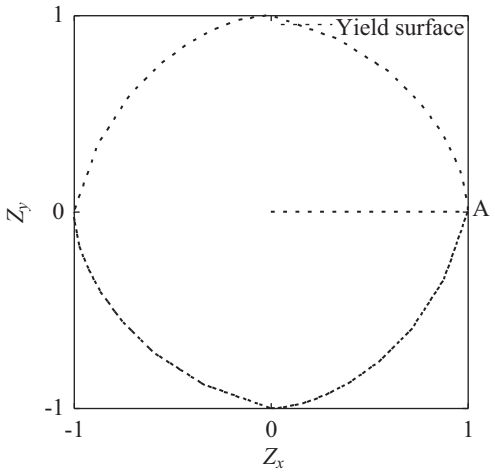
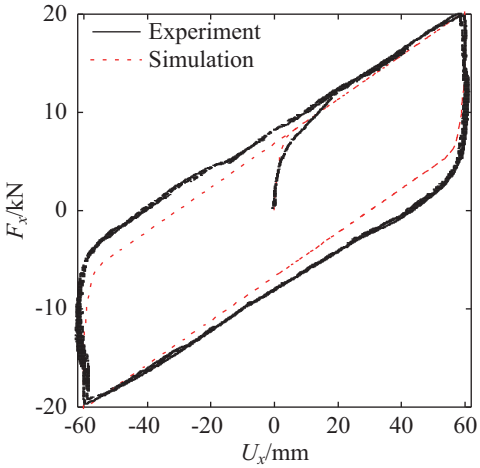
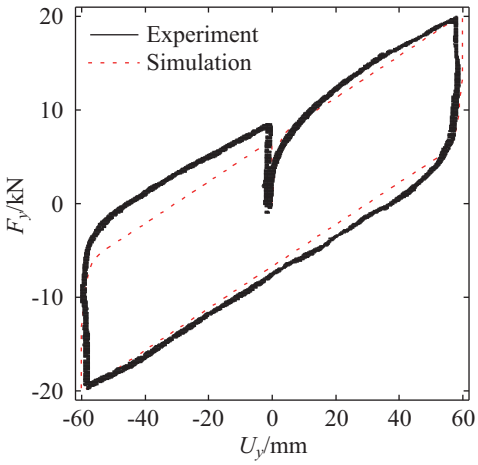


Fig. 6 Simulation response of the hysteretic variable Z.



(a) x direction



(b) y direction

Fig. 7 Comparison of experimental and simulated results of the hysteretic loops.

3.2 Cyclic Tensile Loading Tests and Simulation Analyses

A series of cyclic variable-amplitude tensile loading tests were performed by Warn [31] to characterize the nonlinear behavior of bearings in tension. The bearing had an outer bonded radius of 76 mm and an inner radius of 15 mm, and it consisted of 20 layers of 3 mm thick rubber and 19 layers of 3 mm thick intermediate steel shim, with the thickness of end plate 25 mm. The first shape factor S_1 was 12.2; the second shape factor S_2 was 2.53; the shear modulus of rubbers G was 0.83 MPa; the characteristic strength Q_d was 5.9 kN; and the initial post-elastic stiffness $K_{d,0}$ was 0.398 kN/mm.

As illustrated in Fig. 8, the cyclic tensile loading tests were performed under displacement control with a ramp loading signal, and the bearing was subjected to three sub-cycles with tensile displacement amplitude 6, 30, and 89 mm, respectively, at a loading frequency f of 0.01 Hz.

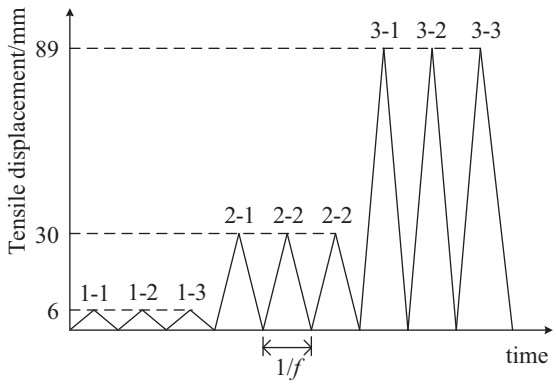


Fig. 8 Ramp loading signal.

https://doi.org/10.1017/jmech.2017.100 Published online by Cambridge University Press

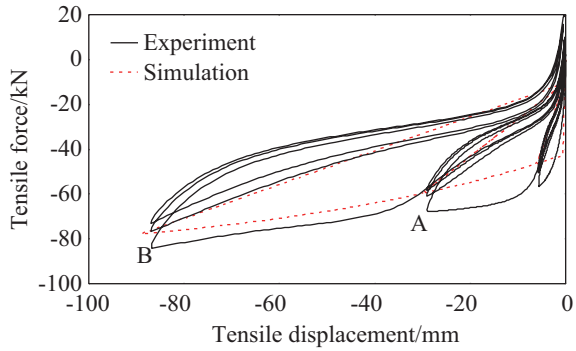


Fig. 9 Comparison of experimental and simulated results for the tensile behavior of bearings.

The experimental and simulation results are plotted in Fig. 9. In the first three sub-cycles (the cycle 1-1, 1-2 and 1-3 in Fig. 8) where the displacement amplitude is 6 mm, the tensile force-displacement response is nearly linear.

In the second three sub-cycles (the cycle 2-1, 2-2 and 2-3 in Fig. 8), as the tensile displacement first reaches 30 mm (point A in Fig. 9) and accordingly exceeds the initial cavitation displacement u_c (in the cycle 2-1), the tension stiffness reduction due to cavitation in rubbers is observed and the subsequent unloading follows a new path. The permanent damage within rubbers is indicated by the area enclosed by the loading and unloading paths. The following loading and unloading (in the cycle 2-2, 2-3) approximately moves along the unloading path experienced in the cycle 2-1, as the displacement in the latter two sub-cycles does not exceed 30 mm, i.e., the current $u_{\max}$.

In the third three sub-cycles (the cycle 3-1, 3-2 and 3-3 in Fig. 8), as the tensile displacement reaches 89 mm (point B in Fig. 9), the loading first moves along the latest unloading path until 30 mm and the general trend of subsequent post-cavitation behavior is consistent with that in the cycle 2-1, and the stiffness is further reduced due to the formulation of new cavities within rubber. With the reverse loading applied, it again moves along a new unloading path (in the cycle 3-1).

It is found that the proposed model can reasonably reproduce the associated stiffness reduction after cavitation and the permanent damage effect in bearings under cyclic tensile loadings, whereas, there are slight differences between the experimental and simulated loading/unloading paths, as the loading path does not exactly coincide with the previous unloading path in experiment (more obvious in the cycle 3-2, 3-3). The determined parameters: $k = 10$, $\alpha = 1$ and $\phi_{\max} = 0.75$ in this proposed model are capable of representing the nonlinear tensile behaviors.

3.3 The Dimension Effect on Mechanical Behaviors of LRBs

Since the insufficient capacity and size of experimental setups, these tested bearings are scale models and relatively smaller than actual ones. The existing specific-purpose experimental data, such as bidirectional coupling tests, vertical stiffness and critical load tests, for large-sized bearings are limited. Whereas, the size of bearings dedicated to tensile tests is relatively large, as the requirements for tensile tests are relatively lower. Therefore, 3D FE models for LRBs with different geometrical sizes are utilized to investigate the influence of dimension effect on these mechanical behaviors considered in this numerical model.

The size of a bearing model is determined by four geometric parameters, i.e., external radius R, internal radius r, first shape factor S_1, and second shape factor S_2, as the thickness of single rubber layer and the number of rubber layers are calculated as: $t_r = (R^2 - r^2)/(2RS_1)$ and $n = 2R/S_2t_r$, respectively. To shed light on the influence of geometrical size of bearings on their mechanical properties, the external diameter varies from 200 mm to 360 mm at the interval of 80 mm, and the ratio of internal diameter to external diameter is reasonably assumed to be 0.2, with the values of S_1, S_2 remaining constant, specifically $S_1 = 25$, $S_2 = 3$. The detailed descriptions of FE bearing models can be found in [9, 20, 31].

These bearing models are subjected to box displacement orbit ($\gamma = 100\%$), and the bidirectional resisting forces results for LRBs with different external diameters are illustrated in Fig. 10. It is indicated that the Casciati model is capable of replicating the bidirectional interaction behaviors of FE models with reasonable accuracy.

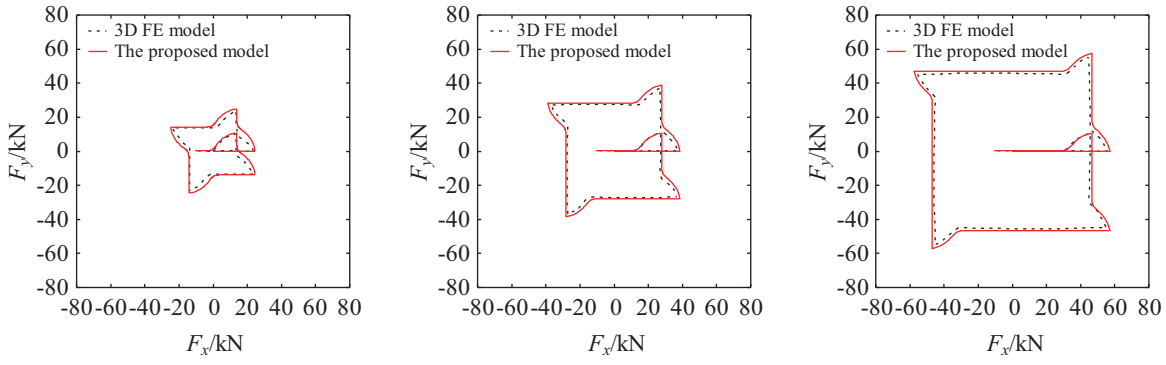
As presented in Fig. 11(a), the post-elastic stiffness is reduced with increasing vertical load, and the normalized results are plotted in Fig. 11(b), with the predicted post-elastic stiffness from Eq. (5) derived from the two-spring model. This comparison indicates that Eq. (5) shows good agreement with FE results and the geometrical size has a negligible impact on the general trend of post-elastic stiffness under varying levels of vertical load.

Figure 12 presents the normalized results for the reduced vertical stiffness in the deformed configuration, with the predicted vertical stiffness from the piecewise linear formulation and the two-spring model, respectively. The piecewise linear method is observed to capture the vertical stiffness at varying levels of lateral displacement more accurately when compared with the two-spring method.

Figure 13 demonstrates the predicted reduction in critical load from the linear reduction method and the overlapping area method, respectively, with the normalized critical load results from FE models with different sizes. It is indicated that the linear reduction method slightly overestimates the critical load at the given lateral offset, with the value of external diameter increasing from 200 mm to 360 mm. Nevertheless, the overlapping area method captures the general trend of critical load observed in the FE results more reasonably.

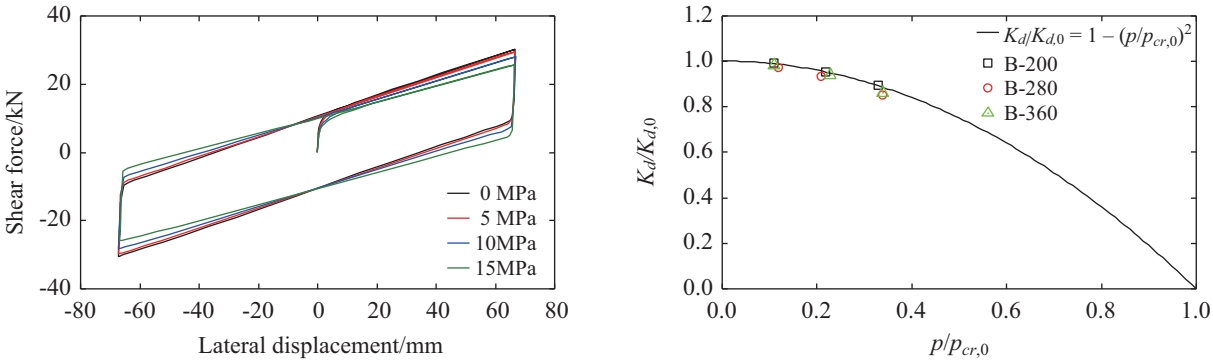
Based on the FE results, it is demonstrated that the dimension effect has a negligible effect on the bidirectional interaction behavior, the reduction in post-elastic stiffness and vertical stiffness. Whereas, the general

https://doi.org/10.1017/jmech.2017.100 Published online by Cambridge University Press



(a) B-200 (b) B-280 (c) B-360

Fig. 10 Comparison of bidirectional resisting forces between FE and predicted results.



(a) The effect of vertical load on post-elastic stiffness for B-200

(b) The results for post-elastic stiffness of bearings with different diameters

Fig. 11 Comparison of post-elastic stiffness between FE results and the two-spring model.

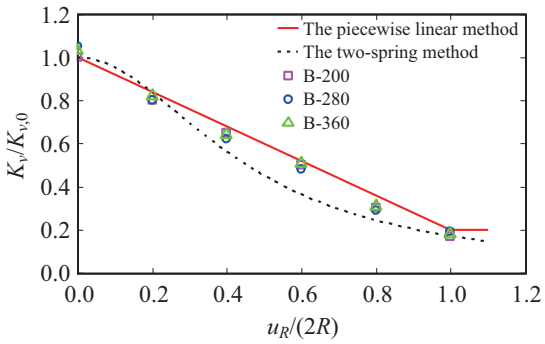


Fig. 12 Comparison of vertical stiffness between FE models and theoretical predictions.

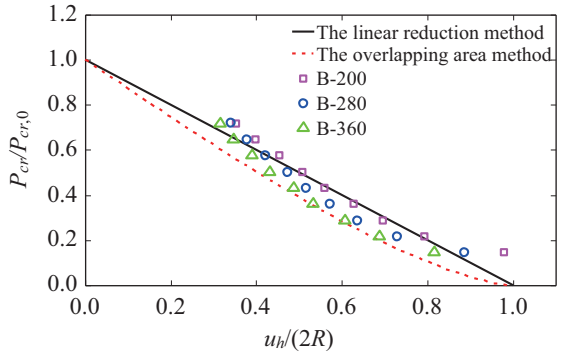


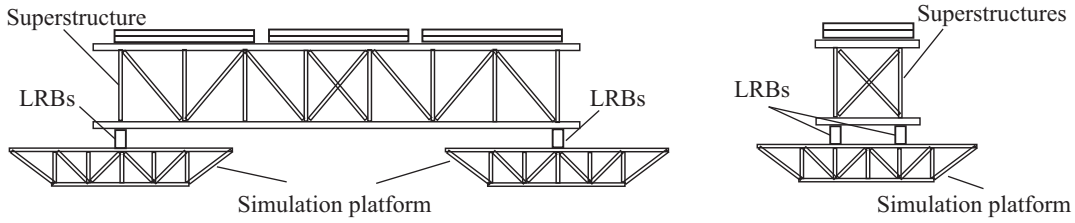
Fig. 13 Comparison of critical load between FE results and theoretical predictions.

trend of critical load of bearings in the deformed configuration is observed to be influenced by their geometrical sizes, and this observation is required to be further validated by full-scale bearing tests. Therefore, the linear reduction method is still utilized to characterize the variation in critical load capacity herein.

3.4 Three-Dimensional Shaking Table Tests and Simulation Analyses

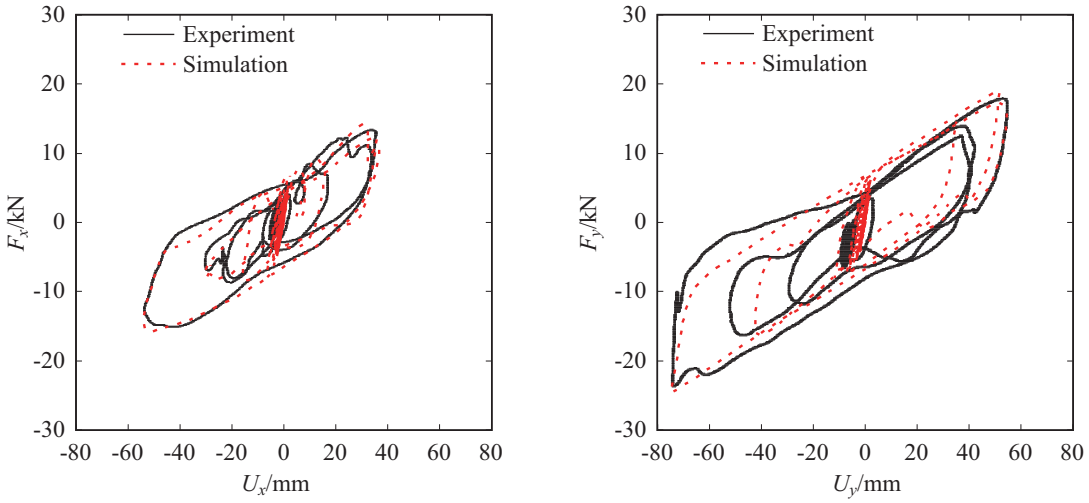
The shaking table tests were conducted on an isolated truss-bridge model by Warn [31] to study the impact of vertical component of seismic excitation on the behav-

https://doi.org/10.1017/jmech.2017.100 Published online by Cambridge University Press



(a) Elevation view (b) Transverse view

Fig. 14 Schematic of the isolated truss-bridge model (Warn [31]).



(a) x direction (b) y direction

Fig. 15 Comparison of experimental and simulated results of the hysteretic loops.

iors of LRBs, and a schematic of the isolated truss-bridge model is illustrated in Fig. 14. This quarter-scale steel-truss superstructure was composed of two parallel planar trusses, and each was 10.7 m in length and 1.5 m in height, with the transverse width 1.2 m. The total weight of the model was approximately 382 kN. The bearings used in this test are identical to those tested under cyclic tensile loadings as outlined above.

3.4.1 Horizontal Behaviors under Dynamic Loadings

The model was subjected to three components of seismic excitation, which were applied in the x, y and z directions simultaneously. This testing was performed at 75% intensity level with a time scale factor of 2. The experimental and simulation responses of individual bearing for the Sylmar-Olive View record (Northridge, 1994) are presented in Fig. 15, it is observed that the numerical model can reasonably reproduce the experimentally observed hysteretic loops over a wide range of lateral displacement level.

As presented in Fig. 16, the plot of the hysteretic variable Z illustrates that the bidirectional coupled response of bearings is incorporated through a circular yield surface, with the hysteretic variable Z bounded by the values of ±1. In Fig. 17, the locus plot of resisting forces in the two orthogonal directions demonstrates that there is a turning-around phenomenon in the horizontal plane near the restoring force of 5 kN.

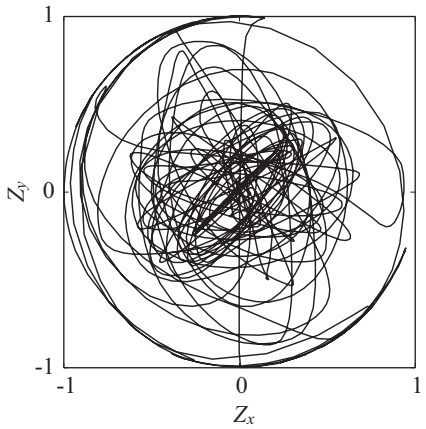


Fig. 16 The locus of hysteretic variable Z.

https://doi.org/10.1017/jmech.2017.100 Published online by Cambridge University Press

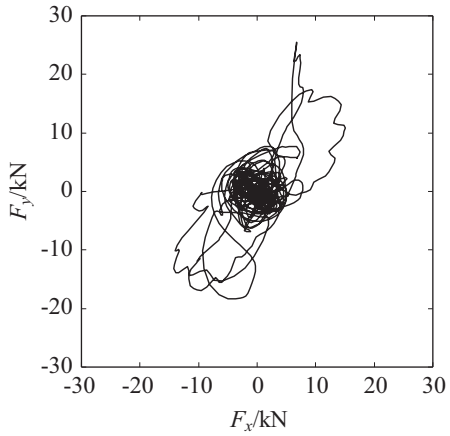
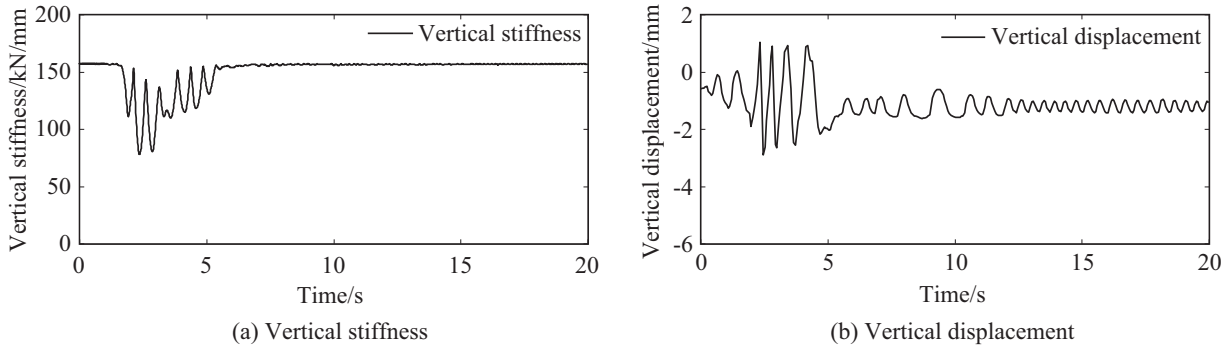


Fig. 17 The locus of restoring forces in the horizontal plane.



(a) Vertical stiffness (b) Vertical displacement

Fig. 18 Time histories of the vertical stiffness and vertical displacement.

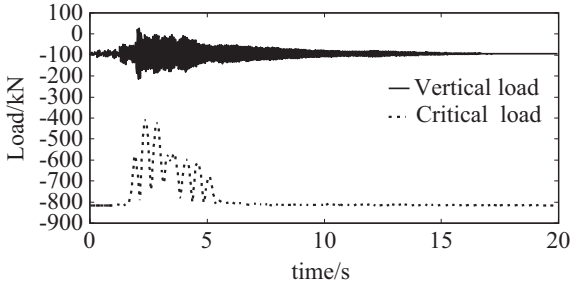


Fig. 19 Time histories of the vertical load and critical load.

Therefore, the numerical model is capable of accurately predicting the bi-lateral coupled effect of LRBs subjected to three-dimensional seismic excitation.

3.4.2 The Performance of LRBs Accounting for the Variation in Vertical Stiffness and Critical Load

When the variation in vertical stiffness and critical load is considered, the performance of bearings is presented herein. The time histories of vertical stiffness and vertical displacement are shown in Fig. 18, and the minimum value of vertical stiffness in the test is 77.716 kN/mm, with the initial vertical stiffness 157.055 kN/mm. The minimum and maximum values of vertical displacement are 1.39 mm and 3.48 mm, respectively, and the decrease in height of bearings may result in the axial load redistribution in the composite isolation system that is composed of LRBs and flat sliding bearings.

From the time history plot of the vertical load and critical load presented in Fig. 19, the maximum value of vertical load is 217.8 kN due to the contribution of over-

https://doi.org/10.1017/jmech.2017.100 Published online by Cambridge University Press

turning forces and vertical component of seismic excitation. It is observed that the bearing does not reach its stability limit state, as the critical load is always greater than the vertical load for this recorded motion. Whereas, the minimum value of critical load is 404.95 kN by comparison with the initial critical load of 818.36 kN.

Therefore, the vertical stiffness and critical load of bearings are reduced substantially during earthquakes, and the current practice neglecting the reduction in both vertical stiffness and critical load in analysis might compromise the evaluation of LRBs performances.

4. CONCLUSIONS

In this study, a numerical model of LRBs is presented and implemented in OpenSees as a user-defined element. The proposed model is a 2-node, 12-degrees-of-freedom macro element, which has the advantages of convenient implementation and computational efficiency. In the horizontal plane, this element accounts for the bidirectional coupled response and the reduction of post-elastic stiffness due to vertical load. In the axial direction of the model, the reduced vertical stiffness and critical load under large lateral displacement are considered, and the effects of cavitation as well as permanent damage in bearings are mathematically incorporated. Simulation analyses are conducted for both static and dynamic loading tests, i.e., bidirectional static tests, cyclic tensile loading tests and three-directional shaking table tests. The rationality of model parameters in this proposed model is evaluated by experimental data, and the performances of bearings are demonstrated when considering the variation in mechanical properties. Main conclusions are made as follows:

(1) Compared with the experimental results, from both static and dynamic loading tests, the numerical model can reasonably represent the bi-lateral interaction behavior of bearings over a wide range of horizontal displacement.

(2) Under cyclic tensile loading tests, the observed nonlinear tensile behaviors, which include the cavitation and permanent damage in bearings, are captured accurately.

(3) From the comparison between FE results and theoretical predictions, the dimension effect is observed to have a negligible effect on the bidirectional coupled effect, the reduction in post-elastic stiffness and vertical stiffness. Whereas, the general trend of critical load capacity observed in FE results is slightly influenced by the size of bearings, and this observation is required to be further validated by full-scale bearing tests.

(4) The vertical stiffness and critical load of bearings are remarkably reduced during severe earthquakes, and the reduced vertical stiffness and critical buckling load capacity might significantly affect the failure mode of LRBs.

(5) The numerical model is beneficial to, more accurately and efficiently, dynamic analyses of seismic isolated high-rise structures. In this case, there are large variations in vertical loads, or even tensile loads, on bearings due to significant overturning forces and vertical component of excitation under moderate to severe earthquakes.

ACKNOWLEDGEMENTS

This research is supported by the National Natural Science Foundation of China (Grant No. 51438002).

NOMENCLATURE

F	Horizontal resisting force;
F_x, F_y	Components of the horizontal resisting force F;
U	Horizontal deformation;
U_x, U_y	Components of the horizontal deformation U;
K_d	Post-elastic stiffness;
Q_d	Characteristic strength;
c_b	Viscous damping coefficient of rubbers;
Z	Dimensional hysteretic variable;
Z_x, Z_y	Components of the hysteretic variable Z;
χ	Transform variable (meaningless);
Y	Yield displacement;
τ	The ratio of the elastic stiffness to the post-elastic stiffness of bearings;
$[I]$	Second-order identity matrix;
sign()	Sign function;
η	The smoothness parameter;
δ, β, A	The parameters determining the shape and scale of the hysteretic loop;
F_p	Hysteretic force;
G_{eff}	Effective shear modulus of the bearings;
$K_{d,0}$	Initial post-elastic stiffness;
A_b	The bonded area of rubber;
T_r	Total thickness of rubber;
n	The number of rubber layers;
t_r	The thickness of single rubber layer;
P	Vertical load;
$P_{cr,0}$	Critical load of the bearings under zero lateral displacement;
R, r	Outer and inner radius of bearings;
$K_{v,0}$	Initial vertical stiffness in the undeformed state;
E_c	The compression modulus of bearings;
S_1	The first shape factor;
K	Bulk modulus of rubber;
λ	Geometric parameter of the bearing;
K_v	Vertical stiffness of the bearings at a given lateral offset;
u_h	Lateral offset;

https://doi.org/10.1017/jmech.2017.100 Published online by Cambridge University Press

P_{cr}	Critical load of bearings in the deformed state;
P_D, P_{SL}, P_{OT}	Vertical load due to dead, seismic-live, overturning forces respectively;
S_2	The second shape factor;
γ	Shear strain;
F_c	Initial cavitation strength;
u_c	Initial cavitation displacement;
G	Shear modulus of the rubber;
k	The cavitation parameter;
$u_{\max}$	Previous maximum tensile deformation;
α	The strength degradation parameter;
$\phi_{\max}$	The damage index;
F_{cn}	The reduced cavitation strength;
K_b, K_r	The bending and torsional stiffness of the bearings;
I_s, J	The bending and polar moment of inertia of the bonded area of rubber;
H	Total bearing height excluding end plates;
f	Loading frequency;

REFERENCES

1. Chimamphant, S. and Kasai, K., "Comparative Response and Performance of Base-Isolated and Fixed-Base Structures," *Earthquake Engineering & Structual Dynamics*, **45**, pp. 5-27 (2016).
2. Huang, Y. N., Whittaker, A. S., Kennedy, R. P. and Mayes, R. L., "Response of Base-Isolated Nuclear Structures for Design and Beyond-Design Basis Earthquake Shaking," *Earthquake Engineering & Structual Dynamics*, **42**, pp. 339-356 (2013).
3. Cardone, D. and Flora, A., "An Alternative Approach for the Seismic Rehabilitation of Existing RC Buildings Using Seismic Isolation," *Earthquake Engineering & Structual Dynamics*, **45**, pp. 91-111 (2016).
4. Chalhoub, M. S. and Kelly, J. M., "Effect of Bulk Compressibility on the Stiffness of Cylindrical Base Isolation Bearings," *International Journal of Solids and Structures*, **26**, pp. 743-760 (1990).
5. Tsai, H. C., "Compression Stiffness of Circular Bearings of Laminated Elastic Material Interleaving with Flexible Reinforcements," *International Journal of Solids and Structures*, **43**, pp. 3484-3497 (2006).
6. Huang, W. H., "Bi-Directional Testing, Modeling, and System Response of Seismically Isolated Bridges," Ph.D Dissertation, Department of Civil and Environmental Engineering, University of California, Berkeley, CA, U.S.A. (2002).
7. Harvey, P. S. and Gavin, H. P., "Truly Isotropic Biaxial Hysteresis with Arbitrary Knee Sharpness," *Earthquake Engineering & Structual Dynamics*, **43**, pp. 2051-2057 (2014).
8. Warn, G. P., Whittaker, A. S. and Constantinou, M. C., "Vertical Stiffness of Elastomeric and Lead–Rubber Seismic Isolation Bearings," *Journal of Structual Engineering*, **133**, pp. 1227-1236 (2007).
9. Weisman, J. and Warn, G. P., "Stability of Elastomeric and Lead-Rubber Seismic Isolation Bearings," *Journal of Structual Engineering*, **138**, pp. 215-223 (2012).
10. Sanchez, J., Masroor, A., Mosqueda, G. and Ryan, K., "Static and Dynamic Stability of Elastomeric Bearings for Seismic Protection of Structures," *Journal of Structual Engineering*, **139**, pp. 1149-1159 (2013).
11. Kumar, M., Whittaker, A. S. and Constantinou, M. C., "Experimental Investigation of Cavitation in Elastomeric Seismic Isolation Bearings," *Engineering Structures*, **101**, pp. 290-305 (2015).
12. Crowder, A. P. and Becker, T. C., "Experimental Investigation of Elastomeric Isolation Bearings with Flexible Supporting Columns," *Journal of Structual Engineering*, **143**, 04017057 (2017).
13. Tubaldi, E., Mitoulis, S., Ahmadi, H. and Muhr, A., "A Parametric Study on the Axial Behaviour of Elastomeric Isolators in Multi-Span Bridges Subjected to Horizontal Seismic Excitations," *Bulletin of Earthquake Engineering*, **14**, pp. 1285-1310 (2016).
14. Koh, C. G. and Kelly, J. M., "A Simple Mechanical Model for Elastomeric Bearings Used in Base Isolation," *International Journal of Mechanical Sciences*, **30**, pp. 933-943 (1988).
15. Ryan, K. L., Kelly, J. M. and Chopra, A. K., "Nonlinear Model for Lead-Rubber Bearings Including Axial-Load Effects," *Journal of Engineering Mechanics*, **131**, pp. 1270-1278 (2005).
16. Yamamoto, S., Kikuchi, M., Ueda, M. and Aiken, I. D., "A Mechanical Model for Elastomeric Seismic Isolation Bearings Including the Influence of Axial Load," *Earthquake Engineering & Structual Dynamics*, **38**, pp. 157-180 (2009).
17. Kikuchi, M., Nakamura, T. and Aiken, I. D., "Three-Dimensional Analysis for Square Seismic Isolation Bearings under Large Shear Deformations and High Axial Loads," *Earthquake Engineering & Structual Dynamics*, **39**, pp. 1513-1531 (2010).
18. Ishii, K., Kikuchi, M., Nishimura, T. and Black, C. J., "Coupling Behavior of Shear Deformation and End Rotation of Elastomeric Seismic Isolation Bearings," *Earthquake Engineering & Structual Dynamics*, **46**, pp. 677-694 (2017).
19. Kumar, M., Whittaker, A. S. and Constantinou, M. C., "An Advanced Numerical Model of Elastomeric Seismic Isolation Bearings," *Earthquake Engineering & Structual Dynamics*, **43**, pp. 1955-1974 (2014).
20. Han, X. and Warn, G. P., "Mechanistic Model for Simulating Critical Behavior in Elastomeric Bearings," *Journal of Structual Engineering*, **141**, 04014140 (2015).

https://doi.org/10.1017/jmech.2017.100 Published online by Cambridge University Press

21. Maureira, N., de la Llera, J., Oyarzo, C. and Miranda, S., "A Nonlinear Model for Multilayered Rubber Isolators Based on a Co-Rotational Formulation," *Engineering Structures*, **131**, pp. 1-13 (2017).
22. Nagarajaiah, S., Reinhorn, A. M. and Constantinou, M. C., "Nonlinear Dynamic Analysis of 3-D-Base-Isolated Structures," *Journal of Structual Engineering*, **117**, pp. 2035-2054 (1991).
23. Park, Y. J., Wen, Y. K. and Ang, A. H-S., "Random Vibration of Hysteretic Systems under Bi-Directional Ground Motions," *Earthquake Engineering & Structual Dynamics*, **14**, pp. 543-557 (1986).
24. *OpenSees V2.5.0* [Computer software]. Pacific Earthquake Engineering Research Center (PEER), University of California, Berkeley, CA, U.S.A. (2006) (Available from: http://opensees.berkeley.edu) [Accessed on March 2017].
25. Ismail, M., Ikhouane, F. and Rodellar, J., "The Hysteresis Bouc-Wen Model, a Survey," *Archives of Computational Methods in Engineering*, **16**, pp. 161-188 (2009).
26. Ikhouane, F. and Rodellar, J., *Systems with Hysteresis: Analysis, Identification and Control Using the Bouc-Wen Model*, 1st Edition, John Wiley & Sons, Chichester, pp. 63-110 (2007).
27. Wen, Y. K., "Method for Random Vibration of Hysteretic Systems," *Journal of the Engineering Mechanics Division*, **102**, pp. 249-263 (1976).
28. Casciati, F., "Stochastic Dynamics of Hysteretic Media," *Structural Safety*, **6**, pp. 259-269 (1989).
29. Buckle, I. G., Constantinou, M., Dicleli, M. and Ghasemi, H., "Seismic Isolation of Highway Bridges," *Rep. No. MCEER-06-SP07*, Multidisciplinary Center for Earthquake Engineering Research, the State University of New York at Buffalo, NY, U.S.A. pp. 51-74 (2006).
30. Fenves, G. L., Huang, W. H., Whittaker, A. S., Clark, P. W. and Mahin, S. A., "Modeling and Characterization of Seismic Isolation Bearings," *Proceedings of the U.S.-Italy Workshop on Seismic Protective Systems for Bridges*, NY, U.S.A. (1998).
31. Warn, G. P., "The Coupled Horizontal-Vertical Response of Elastomeric and Lead-Rubber Seismic Isolation Bearings," Ph.D Dissertation, Department of Civil, Structural and Environmental Engineering, the State University of New York at Buffalo, NY, U.S.A. (2006).
32. *Guide Specificationsfor Seismic Isolation Design*, American Association of State Highway and Transportation Officials (AASHTO), Washington DC, U.S.A. pp. 23-25 (2014).
33. Haringx, J. "On Highly Compressible Helical Springs and Rubber Rods, and Their Application for Vibration-Free Mountings, 3," *Philips Research Reports*, **4**, pp. 206-220 (1949).
34. Kelly, J. M. and Konstantinidis, D. A., *Mechanics of Rubber Bearings for Seismic and Vibration Isolation*, 1st Edition, John Wiley & Sons, New York, pp. 83-110 (2011).
35. Montuori, G. M., Mele, E., Marrazzo, G., Brandonisio, G. and Luca, A. D., "Stability Issues and Pressure–Shear Interaction in Elastomeric Bearings: The Primary Role of the Secondary Shape Factor," *Bulletin of Earthquake Engineering*, **14**, pp. 569-597 (2016).
36. Kumar, M., "Seismic Isolation of Nuclear Power Plants Using Elastomeric Bearings," Ph.D Dissertation, Department of Civil, Structural and Environmental Engineering, the State University of New York at Buffalo, NY, U.S.A. (2015).
37. Gent, A. N., *Engineering with Rubber: How to Design Rubber Components*, 3rd Edition, Hanser Publications, Cincinnati, pp 119-150 (2012)

(Manuscript received April 14, 2017,
accepted for publication October 2, 2017.)

https://doi.org/10.1017/jmech.2017.100 Published online by Cambridge University Press